

# Analysis of Individual Extensive Air Shower using Pulse Shape Information

by

Kamilya Yessimbet

Submitted to the Department of Physics  
in partial fulfillment of the requirements for the degree of

Master of Science in Physics

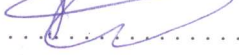
at the

NAZARBAYEV UNIVERSITY

Apr 2018

© Nazarbayev University 2018. All rights reserved.

Author .....  .....  
Department of Physics  
Apr 29, 2018

Certified by .....  .....  
Dmitriy Beznosko  
Assistant Professor  
Thesis Supervisor

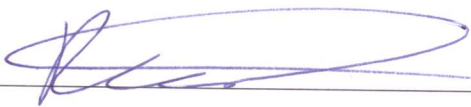
Accepted by .....  .....  
Vassilios D. Tourassis  
Dean, School of Science and Technology

NAZARBAYEV UNIVERSITY SCHOOL OF SCIENCE AND TECHNOLOGY

As members of the Thesis Committee, we verify that we have read the thesis prepared by Kamilya Yessimbet entitled

ANALYSIS OF INDIVIDUAL EXTENSIVE AIR SHOWER USING PULSE SHAPE INFORMATION

and recommend that it be accepted as fulfilling the thesis requirement for the Degree of Master of Science.



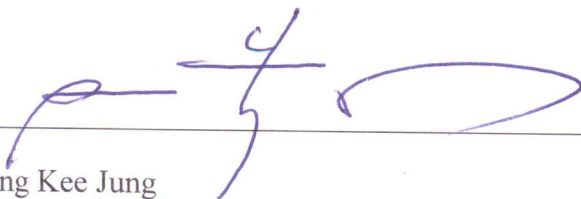
April 23, 2018

Dmitriy Beznosko



April 23, 2018

Vassilios Kovanis

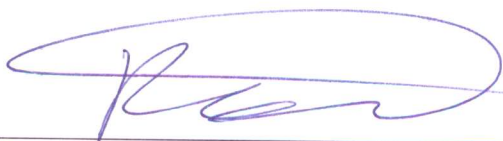


April 23, 2018

Chang Kee Jung

Final approval and acceptance of this thesis is contingent upon the candidate's submission of final copies of the thesis to the Department of Physics.

I hereby certify that I have read this thesis prepared under my direction and recommend that it be accepted as fulfilling the thesis requirement.



April 23, 2018

Thesis Supervisor: Dmitriy Beznosko

# Analysis of Individual Extensive Air Shower using Pulse Shape Information

by

Kamilya Yessimbet

Submitted to the Department of Physics  
on Apr 29, 2018, in partial fulfillment of the  
requirements for the degree of  
Master of Science in Physics

## Abstract

Study of Ultra-High energy Cosmic Rays (UHECR) coming to Earth from the deep cosmos has the potential to open the veil on some remaining mysteries in the field of High Energy Physics and Astrophysics. Horizon-T detector system is constructed to study the nature of UHECR by means of studying its interactions with the Earth atmosphere that result in so-called Extensive Air Showers (EAS). The detector system is based at Tien Shan High-altitude Science Station (TSHSS) of P.N. Lebedev Physical Institute of the Russian Academy of Sciences. It is located near the Almaty city, Kazakhstan, at  $\sim 3400$  meter above the sea level. About 2000 EAS were selected from the Physics Run 1 that has been detected during the period from January 2017 to April 2017 at Horizon-T detector system. The simulation activities indicate the existence of the "invariant" property of the standard EAS as defined by the CORSIKA simulator. In this work, I analyzed single-peaked EAS events in order to use this property as a new approach to EAS data analysis using the fine time resolution feature of Horizon-T detector. The definition of this invariant property, its test using data and the classification of the EAS events from Physics Run 1 are described in this thesis.

Thesis Supervisor: Dmitriy Beznosko  
Title: Assistant Professor

## Acknowledgments

I would like to thank my scientific adviser Dmitriy Beznosko for the guidance and support. This work in part was supported by NU Center of Excellence, MES RK state-targeted program BR05236454.

# Contents

<b>1</b>	<b>Introduction</b>	<b>10</b>
1.1	Cosmic rays . . . . .	11
<b>2</b>	<b>Extensive Air Showers</b>	<b>12</b>
2.1	Hadronic interactions . . . . .	13
2.1.1	Electromagnetic interactions . . . . .	14
2.1.2	Muonic interactions . . . . .	16
<b>3</b>	<b>EAS Simulation and Analysis</b>	<b>18</b>
3.1	EAS structure and development . . . . .	18
3.1.1	Longitudinal development . . . . .	18
3.1.2	Lateral development . . . . .	20
3.1.3	Random walk . . . . .	22
3.2	Simulation results . . . . .	24
<b>4</b>	<b>Experiment Physics Run 1</b>	<b>28</b>
4.1	HorizonT detector system . . . . .	28
4.2	Data analysis and classification . . . . .	30
4.2.1	Standard EAS . . . . .	31
4.2.2	Testing and verification of simulation results on data . . . . .	34
4.2.3	Multimodal EAS . . . . .	36
4.2.4	Statistics . . . . .	40
<b>5</b>	<b>Conclusion</b>	<b>42</b>

<b>A Tables</b>	<b>44</b>
<b>B Figures</b>	<b>45</b>

# List of Figures

2-1	The scheme of longitudinal and lateral development of EAS [1]. . . . .	12
2-2	Shower disk arriving at the ground [1] . . . . .	13
3-1	Particle densities of the EAS longitudinal development relative to the atmospheric depth [2]. . . . .	19
3-2	Arrival time vs. distance from the EAS axis. . . . .	20
3-3	Electrons arrival at 50 meters from the core. . . . .	21
3-4	Electrons arrival at 110 meters from the core. . . . .	21
3-5	Peak width vs. distance from the EAS axis. . . . .	22
3-6	Arrival time vs. distance from the core. . . . .	23
3-7	Invariant property $\rho^{0.5}(R) * \tau(R)$ of simulated EAS (proton and Fe primaries) vs. distance from the EAS axis [3]. . . . .	25
3-8	Invariant property $\rho^{0.5}(R) * \tau(R)$ of simulated EAS (proton and Fe primaries) vs. distance from the EAS axis [3]. . . . .	25
3-9	Test on $\rho^{0.5}(R) * \tau(R)$ for EAS arriving at different angles vs. distance from the EAS axis [3]. . . . .	26
3-10	Test on $\rho^{0.5}(R) * \tau(R)$ for EAS arriving at the detector of size $2 \times 2 m^2$ [3]. . . . .	27
4-1	Top view of Horizon-T detector system. . . . .	28
4-2	Illustration of basic SC detector operation. . . . .	30
4-3	Single pulse of EAS detected at HT detector system. . . . .	31
4-4	Standard EAS event with all detector channels displayed. . . . .	32
4-5	Standard EAS event without highest peak displayed. . . . .	32

4-6	Peak area or density of particles vs. the distance from the EAS core.	33
4-7	Peak width vs. distance from the EAS core. . . . .	33
4-8	Test on invariance of $\rho^{0.5}(R) * \tau(R)$ in EAS event . . . . .	35
4-9	Test on invariance of $^{0.5}(R) * \tau(R)$ in EAS event. . . . .	36
4-10	MME detected by HT detector system with all channels displayed. . .	37
4-11	MME detected by HT detector system at $\sim 300$ meters from axis. . .	38
4-12	MME detected by HT detector system at $\sim 500$ meters from axis. . .	38
4-13	Sample MME event with all channels displayed. . . . .	39
4-14	Sample MME event without largest peak. . . . .	40
4-15	Statistics of MME and Standard EAS events detected at HT detector system. . . . .	41
B-1	Sample of MME event with all channels displayed. . . . .	45
B-2	Sample of MME event without largest peak. . . . .	46
B-3	Sample of MME with all channels displayed. . . . .	47
B-4	Sample of MME event without largest peak. . . . .	47



# List of Tables

4.1	HT detector points coordinates. . . . .	29
-----	---	----

# Chapter 1

## Introduction

Cosmic Rays are highly energetic particles that reach the Earth coming from the outer space outside the Solar System.

Cosmic rays were first discovered by V. F. Hess in 1912 with the usage of electrometer lifted up in a balloon to the altitude of 5000 meters [4]. He observed that the level of ionizing radiation is higher at a greater altitude in the atmosphere and concluded that the source of the radiation is in the outer space [5].

Important stages in the development of study of cosmic rays were discoveries of Geiger-Müller counters by H. Geiger and coincidence technique by W. Bothe and W. Kolhöster in 1920s [6]. They were crucial for the discovery of extensive air showers. In 1927, D. Skobeltsyn made a photograph of tracks left by cosmic rays in a cloud chamber. Cloud chamber experiments led to discoveries of the positron in 1932, and later, in 1937 of the muon by C. Anderson. These discoveries gave a birth to the particle physics.

In 1938, W. Kolhöster observed coincident signals in Geiger-Mueller tubes, and concluded that the tubes were hit by the showers of secondary particles initiated by a primary cosmic particle in the atmosphere. Later, P. Auger held experiment in Alps at the altitude of 3500 m and observed coincidence between two detectors separated by large distances [5]. As W. Kolhöster, P. Auger came to conclusion that registered particles were generated in the atmosphere and originated from a single cosmic ray particle.

Since then, the intensive study of cosmic rays showers or later called extensive air showers (EAS) has started. First experiments on study of EAS structure were held Bruno Rossi in the USA and G. Zatsepin in Russia. Many installations of detector systems were built around the world (Fly's Eye, AGASA, Yakutsk, HiRes, Pierre Auger Observatory, KASCADE and etc).

## 1.1 Cosmic rays

Cosmic rays are detected in a wide range of energies from  $\sim 10^{10}$  eV up to  $\sim 10^{20}$  eV with the intensity spectrum following a power law

$$dN/dE \sim E^\gamma, \quad (1.1)$$

where  $\gamma$  is the spectral index which is approximately 2.7 for most of the range [5]. Cosmic radiation includes "primary" particles and "secondaries" that are produced as the result of interaction of primary particles with interstellar matter. The primary particles are created by various processes in astrophysical sources.

Ultra-High energy Cosmic Ray (UHECR) is a name that I will use for the cosmic rays with energies above  $\sim 10^{16}$  eV. It is known that UHECR propagate through the Milky Way experiencing multiple deflected by galactic magnetic fields that cause random orientation of arrival direction. UHECR of energy above  $\sim 10^{18}$  eV are assumed to have extra-galactic origin as galactic magnetic fields do not have strength to contain these particles; however, no certain data exists to support this assumption [5].

The study of cosmic rays has contributed to the development of particle physics. As there are still remaining mysteries about the nature of cosmic rays, the studies of cosmic rays may contribute to further development in this field. Searches for the origin of cosmic rays can lead to our knowledge of the most violent processes that occur in cosmos.

# Chapter 2

## Extensive Air Showers

A primary particle entering the atmosphere initiates creation of a giant shower of particles produced in different multiple interactions that include scattering, decays, pair creation, bremsstrahlung and others. Large number of these particles superimpose and form a single giant cascade that is called Extensive Air Shower (EAS). EAS initiated from a single primary particle is demonstrated in Figure 2-1.

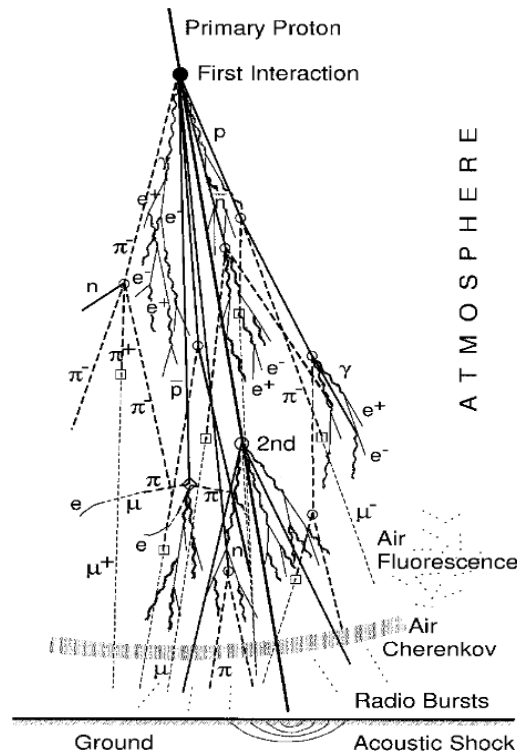


Figure 2-1: The scheme of longitudinal and lateral development of EAS [1].

EAS developing through the atmosphere is accompanied with Air Cherenkov emission, radio emission and air fluorescence.

When EAS reach the Earth, its shower front has a shape of disk (see 2-2). The central region of EAS that is along the axis of shower is called shower axis.

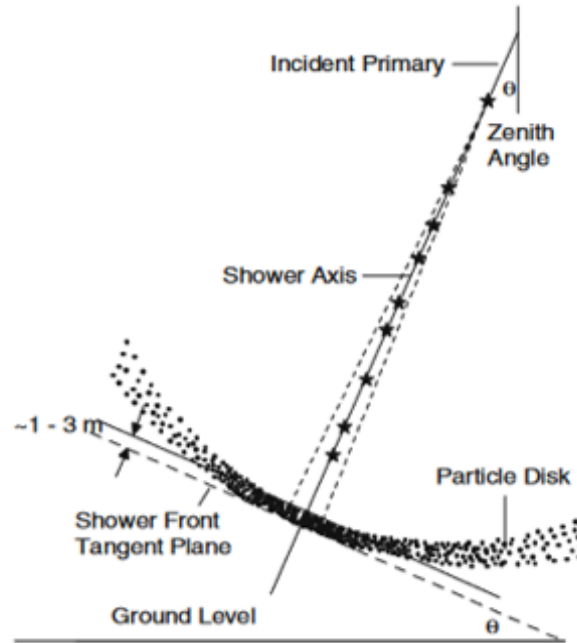


Figure 2-2: Shower disk arriving at the ground [1] .

## 2.1 Hadronic interactions

A primary particle, for example a proton or nucleus, collides with the nuclei of oxygen or nitrogen atoms in the atmosphere, and cause creation of a multitude of secondary particles via hadronic interaction. Other hadronic particles as pions, kaons, protons and neutrons can also be created.

$$p + A = N + (N + \dots + N) + \pi^{\pm 0} + \pi^{\pm 0} \dots + \pi^{\pm 0} \quad (2.1)$$

The number of particles created in the first interaction depends on the energy of incoming particle but typically is about few thousand in the first act. Majority of the

secondaries are pions ( $\sim 90\%$ ) as particles are born with a probability  $\sim 1/m^2$ , with Kaons being  $\sim 10\%$  and all others being a fraction of a percent. Hadronic particles form the EAS core. Charged pions with an every below critical decay and contribute to the muonic component of EAS.

$$\pi^+ \rightarrow \mu^+ + \nu_\mu \quad (2.2)$$

$$\pi^- \rightarrow \mu^- + \bar{\nu}_\mu \quad (2.3)$$

Neutral pions almost immediately decay ( $\tau_{\pi^0} = 0.84 * 10^{-16} s$ ) into gamma photons, which contribute to the development of electromagnetic cascade (EM).

$$\pi^0 \rightarrow \gamma + \gamma \quad (2.4)$$

Kaons can also undergo decays that contributes to hadronic and muonic cascades [2].

$$K^+ \rightarrow \mu^+ + \nu_\mu \quad (2.5)$$

$$K^\pm \rightarrow \pi^\pm + \pi^0 \quad (2.6)$$

$$K^- \rightarrow \mu^- + \bar{\nu}_\mu \quad (2.7)$$

Hadronic cascade propagates along the axis of EAS and contributes to the formation of EM and muonic shower components.

### 2.1.1 Electromagnetic interactions

Charged particles, mainly electrons and positrons, as well as photons are responsible for electromagnetic interactions in the atmosphere forming the electromagnetic component of EAS.

Main electromagnetic interactions: pair production, Compton scattering, photoelectric effect, Coulomb scattering, bremsstrahlung, Cerenkov radiation. Gamma photons born in a decay of neutral pions most probably undergo electron pair pro-

duction or Compton scattering.

When the energy of a photon is above  $50MeV$  it more probably can create an electron pair. It is at least of twice mass of two electrons ( $\sim 1.22MeV$ ) to produce a pair that each particle carries away equal and half energy of the photon energy.

$$\gamma \rightarrow e^+ + e^- \quad (2.8)$$

Electrons and positrons can annihilate and produce two gamma photons.

$$e^+ + e^- \rightarrow \gamma + \gamma \quad (2.9)$$

When a high-energy electron scatters, it changes its direction and is accelerated. This causes the emission of high-energy photons, which is called brehmsstrahlung. If the emitted photons carry energy  $> 1.22$  MeV, then they also can produce electron pair. At energy lower than 1.22 MeV, the Compton scattering mainly occur, when the incident photon scatters with an electron of an atom. At higher energies, Compton scattering and collisions can be neglected.

Electromagnetic showers can be approached using Heitler's simplified model that predicts important features of cascade development [7]. According to the Heitler's model, particles ( $e^+, e^-$  and photons) undergo repetitive two-body splittings in the interaction with the atmosphere. After each interaction, two particles travel a fixed distance  $\lambda_{EM}$  through the atmosphere and carry the half energy of the initial particle. Thus, after  $n$  interactions, the number of particles in the shower will be proportional to  $2^n$ . Produced particles propagating through a certain depth  $X$  in the atmosphere reach a certain number than can be presented as follows

$$N(X) = 2^{\frac{X}{\lambda_{EM}}} \quad (2.10)$$

The multiplication of particles continue until they reach the critical energy  $E_c$ , after which collisional energy losses exceed radiative energy losses. At the critical energy,

EM cascades reaches its maximum number of particles  $N_{max}$ . So that

$$N_{max} = \frac{E_0}{E_c}, \quad (2.11)$$

where  $E_0$  - energy of an initial particle,  $E_c$ - critical energy. When EM cascade reaches its maximum size at the critical energy  $E_c$ , the maximum atmospheric penetration depth is

$$X_{max} = \lambda_{EM} \log_2 \left( \frac{E_0}{E_c} \right), \quad (2.12)$$

This gives us important information of EM cascade development. The Heitler's model predicts shower size that is proportional to  $E_0$ . It also describes logarithmic increase of maximum atmospheric depth of propagation with the energy of a primary particle.

Propagation of charged particles is accompanied by radiation phenomena such as Cherenkov radiation, fluorescence, radio emission, which all are part of electromagnetic cascade [2]. Radiation and ionization are the main processes that cause the loss of energy of electrons and positrons.

### 2.1.2 Muonic interactions

Weakly interacting particles - neutrinos, mostly escape detection. Multiple production of muons occurs as the result of decays of hadronic particles.

According to (2.2) and (2.3), in each decay charge pion produces the muon. Following the simple model of EAS development, the total number of muons will be

$$N_\mu = (N_{ch})^n, \quad (2.13)$$

where  $N_\mu$  - number of muons;  $N_{ch}$  - number of charged pions; n-number of decays. The decay energy of charge pions can be defined as following:

$$E_{dec} = \frac{E_0}{(N_\pi)^n}, \quad (2.14)$$

where  $E_0$  - energy of a primary particle;  $N_\pi$  - total number of pions including neutral.



From  $\ln N_\mu = n \ln N_{ch}$ ,

$$N_\mu = (N_{ch})^n = \left(\frac{E_0}{E_{dec}}\right)^\beta, \quad (2.15)$$

where  $\beta = \ln N_{ch} / \ln N_\pi \approx 0.85$ . Thus,  $N_\mu$  linearly increases with the energy of a primary particle.

Most of muons reach the Earth. Charged muons can contribute to the development of electromagnetic component of EAS.

$$\mu^- \rightarrow e^- + \bar{\nu}_e + \nu_\mu \quad (2.16)$$

$$\mu^+ \rightarrow e^+ + \nu_e + \bar{\nu}_\mu \quad (2.17)$$

# Chapter 3

## EAS Simulation and Analysis

### 3.1 EAS structure and development

In this chapter, EAS characteristic properties as EAS particles density, arrival time and thickness of an EAS disk are studied using EAS models simulated by CORSIKA simulator [8]. Section 3.1.1 discusses longitudinal development of an EAS, and section 3.1.2 discusses its lateral development.

The axis of shower can be defined as propagation of momentum vector of incident particle along the direction of longitudinal development of an EAS. Direction of propagation of primary particle is characterized by two angles, zenith and azimuthal angles, which can be determined experimentally by using EAS arrival time.

#### 3.1.1 Longitudinal development

When an EAS develops through the Earth's atmosphere, number of secondary particles grows exponentially and reduces at the sea level. Particle density distribution is dependent on the energy of a primary particle that can be calculated knowing the radius of an EAS. Shower radius can be determined knowing the particle density.

If to consider the atmosphere cut into slices of thickness of  $20g/cm^2$ , number of particles in each atmospheric slice will characterize the longitudinal development of the EAS, which is demonstrated in Figure 3-1. Here particle density distribution of

100 EAS of the energies  $10^{17} - 10^{20}$  eV simulated by CORSIKA simulator is shown [8, 2].

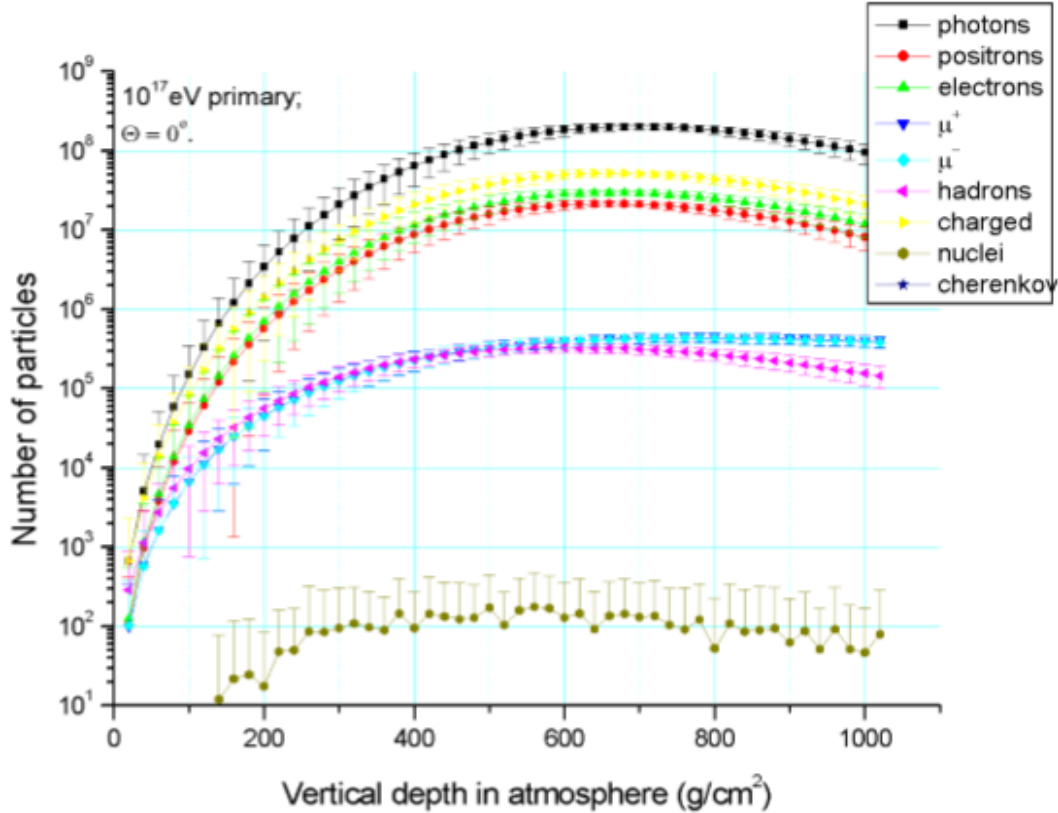


Figure 3-1: Particle densities of the EAS longitudinal development relative to the atmospheric depth [2].

You can see the density distribution of hadrons, electrons, positrons, gammas, muons and charged particles. All these particles are created in multiple interactions in the atmosphere and cause formation of three main shower components described in previous section (hadronic, electromagnetic, muonic). Gamma photons, whose density is sufficiently large, are invisible for the detectors. Muons and contributes a small part to the total number of particles in a single EAS. As the result of multiple interaction, hadrons and charged particles decay and contribute to electromagnetic and muonic EAS components. Thus, only electrons and positrons are used for the analysis purpose.

### 3.1.2 Lateral development

Lateral development of EAS at high-altitude mountain levels can cover large areas (up to a few kilometers), which is dependent of energy of a primary particle or EAS size. An average EAS has laterally symmetry about axis of shower. EAS of low energies are deflected by the magnetic field of Earth, which leads to perturbation of lateral symmetry.

At far distances from the core, low energy particles of muonic and electromagnetic components dominate in the shower. Particle density drops with increase of the radial distance from the EAS axis as  $1/r^2$ , which is demonstrated in Figure 3-2.

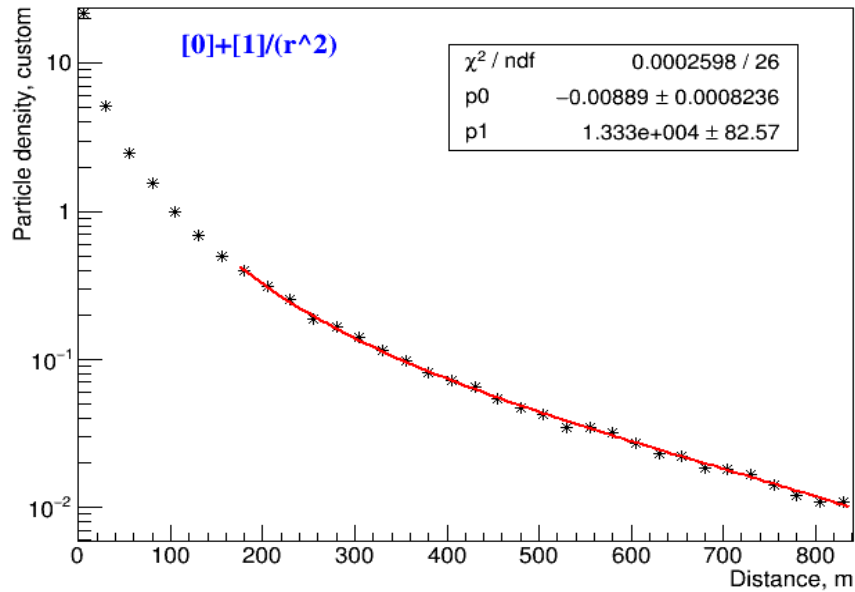


Figure 3-2: Arrival time vs. distance from the EAS axis.

Another EAS characteristic suggested by simulation is widening of an EAS disk that can be defined as a difference in the passage time of an EAS disk. Figures 3-3 and 3-4 illustrate the disk widening at the distances of 50 and 110 meters from the EAS axis respectively. You can see in Figure 3-3 that electrons arrive at the time interval between 75620 ns and  $\sim 75780$  ns. In Figure 3-4, the time interval ends at  $\sim 75900$  ns.

Difference in the disk arrival time is defined as the peak width of EAS particles arrived at a certain detector area.

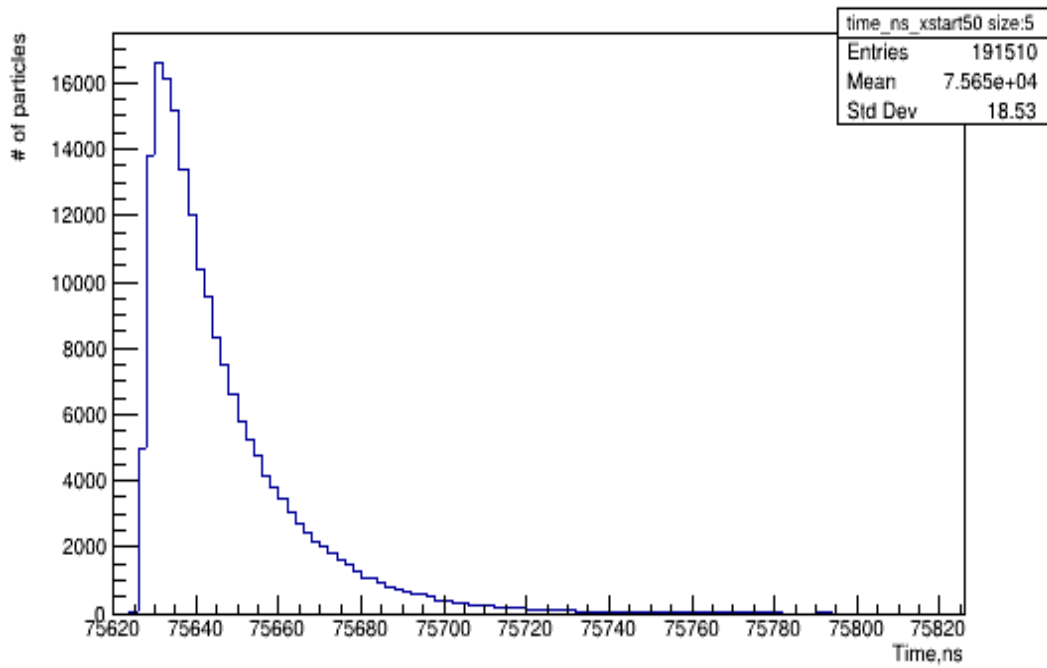


Figure 3-3: Electrons arrival at 50 meters from the core.

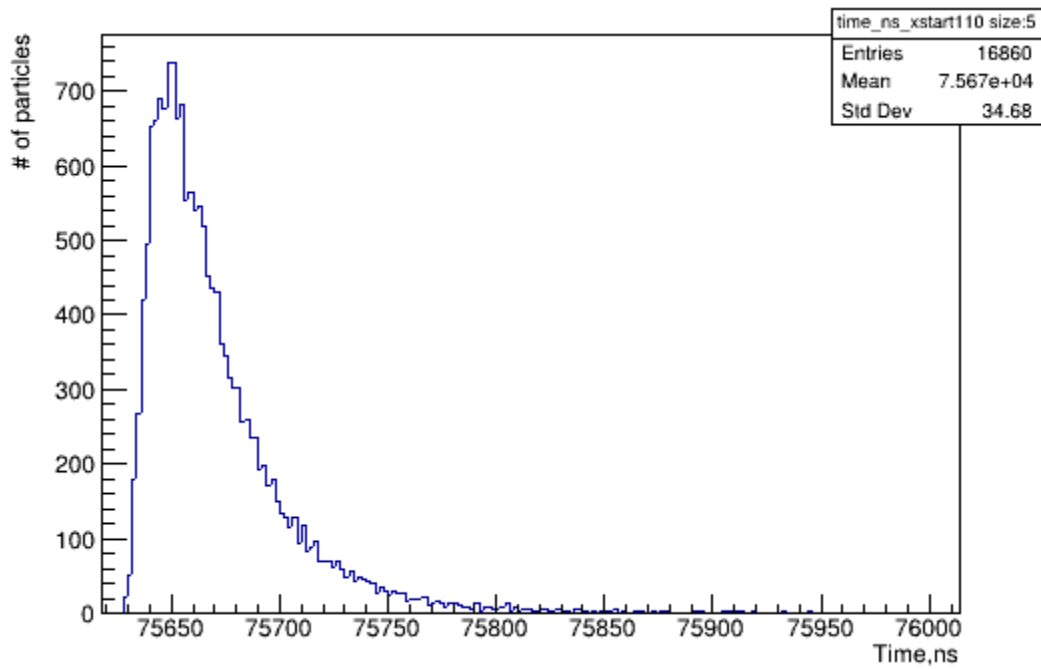


Figure 3-4: Electrons arrival at 110 meters from the core.

In Figure 3-5, it is seen that thickness of the disk linearly increases from the EAS axis.

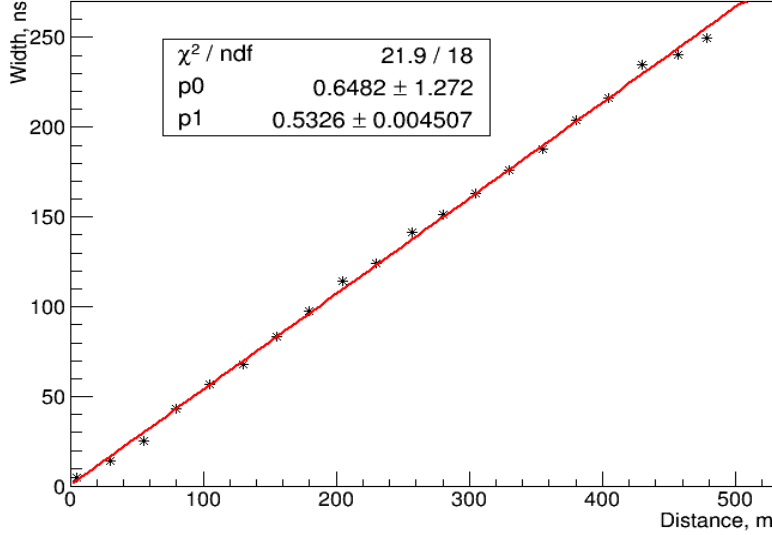


Figure 3-5: Peak width vs. distance from the EAS axis.

### 3.1.3 Random walk

As an EAS disk arrives at the ground, it experiences delay with the increase of the radial distance from the axis.

The delay occur as the result of the increase of number of scattering processes of particles in the atmosphere and as the result of fluctuations in propagation along their path. Since the trajectories of particles become random, their motion is approaching Brownian in nature. According to the theory of Brownian motion or Random walk, the displacement increases as square root of time. The trajectory of a random particle in a shower is described by [9]

$$x_{rms} = \sqrt{\langle x^2(t) \rangle} = \sqrt{\alpha * t}, \quad (3.1)$$

where  $x_{rms}$  - root mean square displacement of a particle undergoing random motion,  $t$  - time,  $\alpha$  - coefficient. In the other words, root mean square function of the prop-

agation displacement of a particle undergoing random process is proportional to the square root of time. Passage time of a particle in the shower is proportional to the radial displacement from the EAS disc axis:

$$t_{arrival} \sim \langle x^2(t) \rangle \quad (3.2)$$

Thus, distribution of disk arrival times increases as  $r^2$  with the distance from the axis. This relation is confirmed by simulator and demonstrated in Figure 4-3.

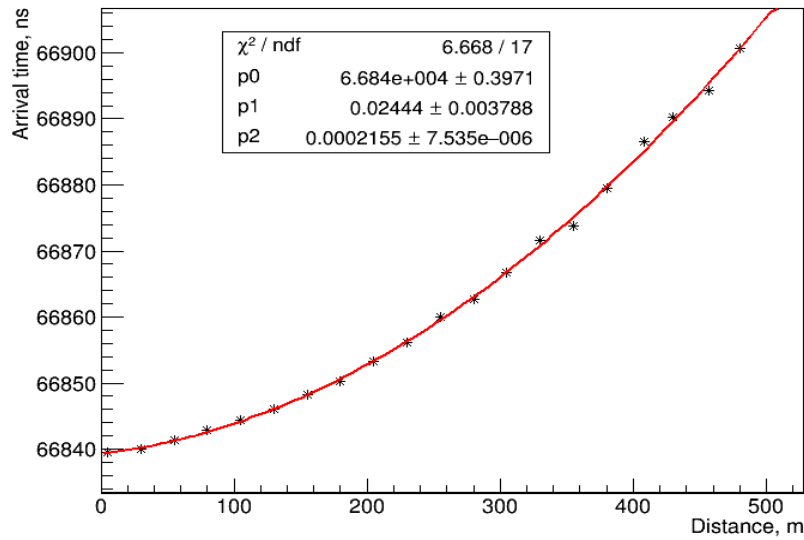


Figure 3-6: Arrival time vs. distance from the core.

According to the above-mentioned EAS characteristics, particle density  $\rho$  drops as  $1/r^2$ , where  $r$  is the distance from the EAS axis. Since time  $t_{arrival}$  is proportional to distance axis as  $r^2$  (Eq. 3.2),  $\rho$  can be defined using  $t_{arrival}$ . Let us define arrival time as  $\tau(R)$ . Following from Eq. 3.2:

$$\frac{1}{\rho(R)} = \sqrt{\alpha \cdot \tau(R)}, \quad (3.3)$$

where  $\alpha$  is a constant value. Thus, the following can be obtained:

$$\sqrt{\rho(R)} \cdot \tau(R) = \frac{1}{\alpha} \quad (3.4)$$

## 3.2 Simulation results

Formation of EAS is a complex process that involve various fundamental interactions and random processes. In this thesis, experimental data obtained at HT detector system is studied and compared with simulation results. In the analysis of simulated EAS, such characteristics as density, energy, time structure and their relations were studied.

Simulations of 10 showers of proton and Fe nucleus primary particles with energy  $10^{16}$  eV were analyzed. It was observed that all simulated EAS events have a single-mode pulse shape, which will be later important in defining EAS types from data.

As the result, the invariant property of EAS was predicted from the theory of Random walk [9, 10]:

$$\rho^{0.5}(R) * \tau(R) = const, \quad (3.5)$$

where  $\rho$  - particle density,  $\tau(R)$  - arrival time of particles. The value  $\rho^{0.5}(R) * \tau(R)$  is dependent on energy of EAS. This property is observed at the distance interval between around 200 and 450 meters from EAS axis, which is demonstrated in Figure 3-7. You can see that at the distance  $> 450$  meters the spread of this value is large and invariant is not observed - this is due to a low particle density at such distances and inaccuracy in pulse width determination. In Figure 3-8, it can be clearly seen that the tested invariant property is valid at the distance interval from  $\sim 200 - 450$  meters.

Simulation was also obtained for both types of primary particles (Fe and proton) of energy  $10^{16}eV$  arriving at 7 different zenith angles ( $0^0, 10^0, 15^0, 30^0, 45^0, 60^0$  and  $75^0$ ). These EAS were tested on invariant property and compared with each other. The results showed that the invariant of  $\rho^{0.5}(R) * \tau(R)$  is observed at the distance interval of  $\sim 200-450$  meters from the axis for of all EAS regardless of the arrival azimuthal angle and is dependent on energy of the primary only (Figure 3-9).

The results discussed above were obtained in simulation of EAS detection at detector of size  $10 \times 10m^2$ . In order to obtain comparison with experimental data, EAS of the same energy ( $10^{16}eV$  and primaries (Fe and proton) were simulated for the de-



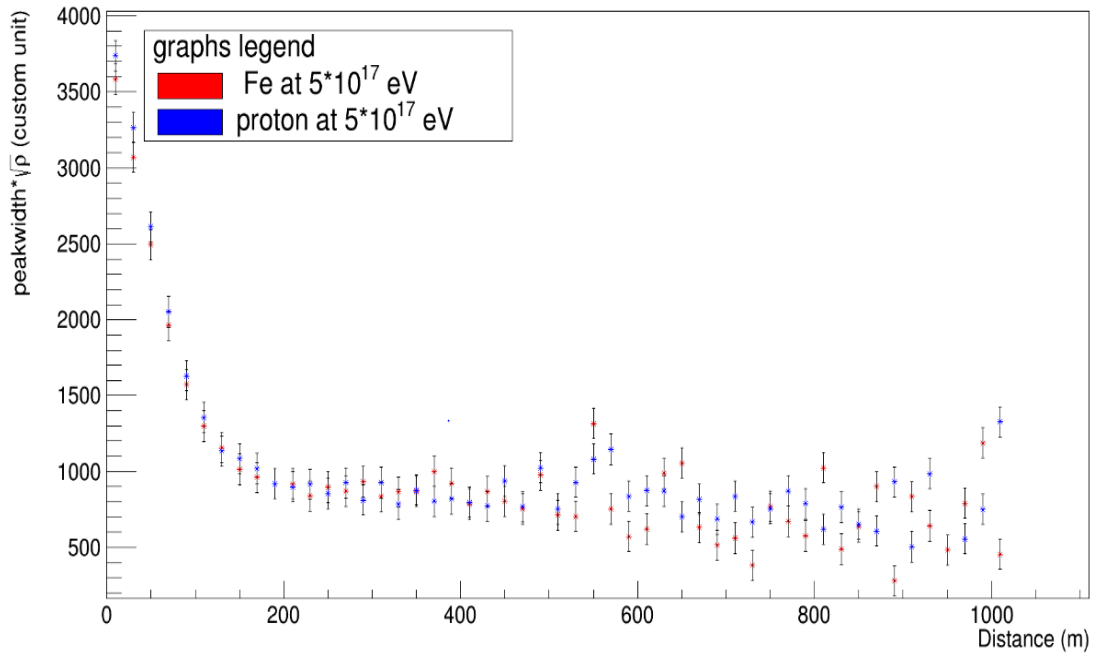


Figure 3-7: Invariant property  $\rho^{0.5}(R) * \tau(R)$  of simulated EAS (proton and Fe primaries) vs. distance from the EAS axis [3].

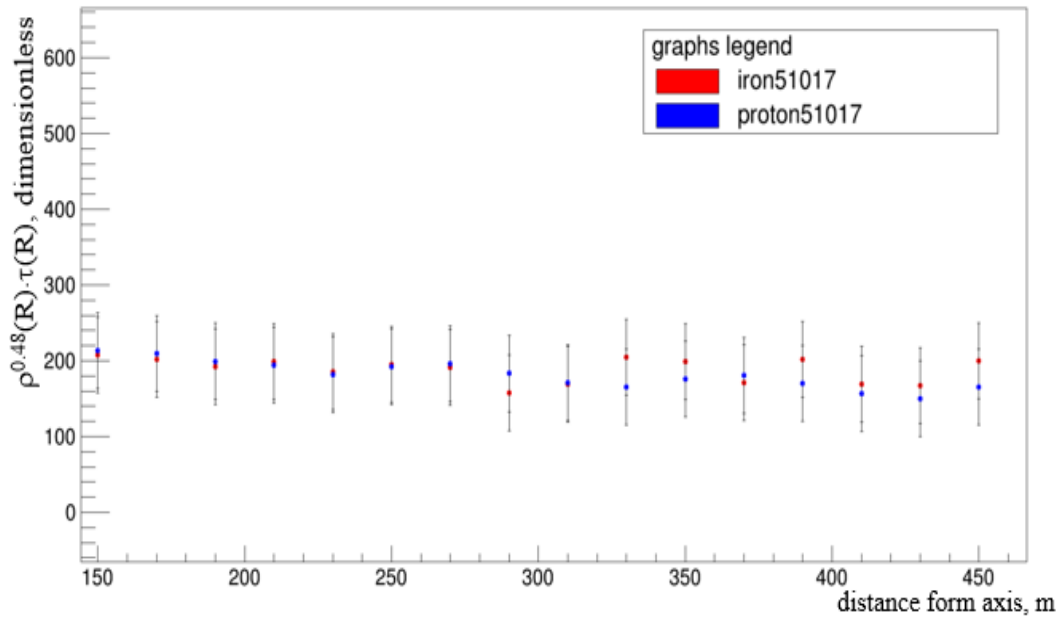


Figure 3-8: Invariant property  $\rho^{0.5}(R) * \tau(R)$  of simulated EAS (proton and Fe primaries) vs. distance from the EAS axis [3].

tector of size  $2 \times 2m^2$ , which is similar to the real detector size at the HT detector system. However, simulation for this detector option did not suggest any possible invariant property. This is illustrated in Figure 3-10.

### Simulation Summary

Simulation of ten EAS events initiated two types of primary cosmic ray particles (Fe and proton) of energy of  $10^{16}$  eV with variation of arrival angles and detector sizes ( $10 \times 10m^2$  and  $2 \times 2m^2$ ) were obtained.

Using the relations of EAS characteristics discussed in Section 3.1, simulated EAS were tested on the invariant property  $\rho^{0.5}(R) * \tau(R)$  that was derived from the theory of Random walk. As the result, this theoretical suggestion was confirmed only for simulation of EAS using detector of size  $10 \times 10m^2$ . The value of  $\rho^{0.5}(R) * \tau(R)$  observed to be relatively constant only at the distance interval of 200 - 450 meters from the EAS axis. It was also shown that invariance of this property depends on the arrival angle of EAS arrival.

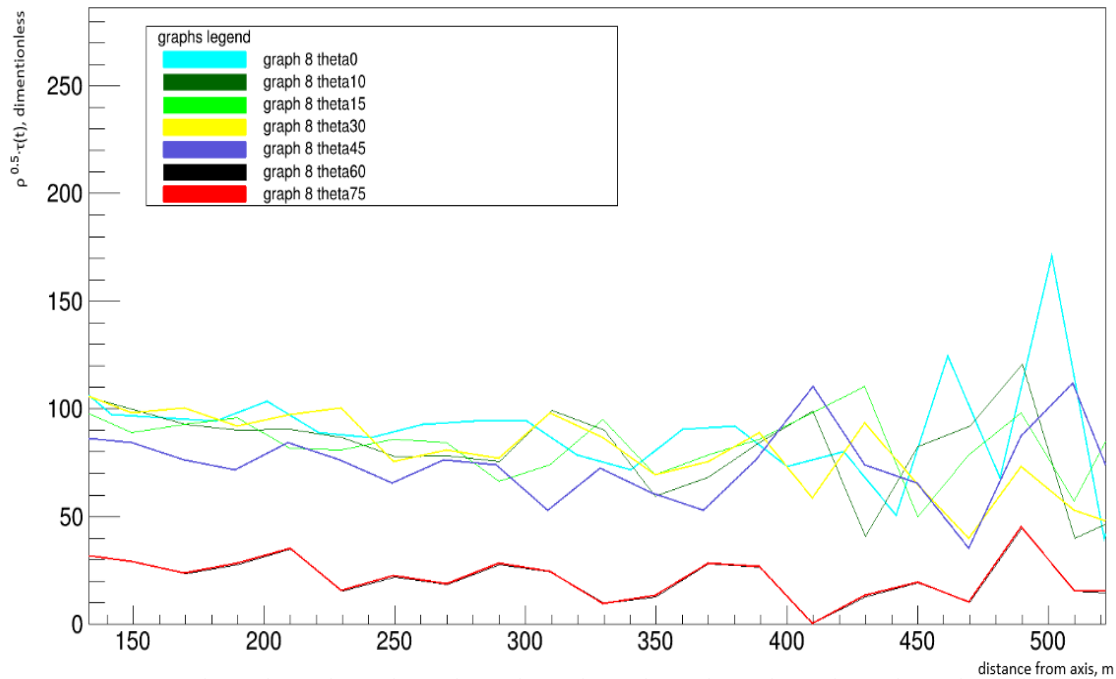


Figure 3-9: Test on  $\rho^{0.5}(R) * \tau(R)$  for EAS arriving at different angles vs. distance from the EAS axis [3].

When an EAS is inclined at a certain angle the invariant property is not being observed.

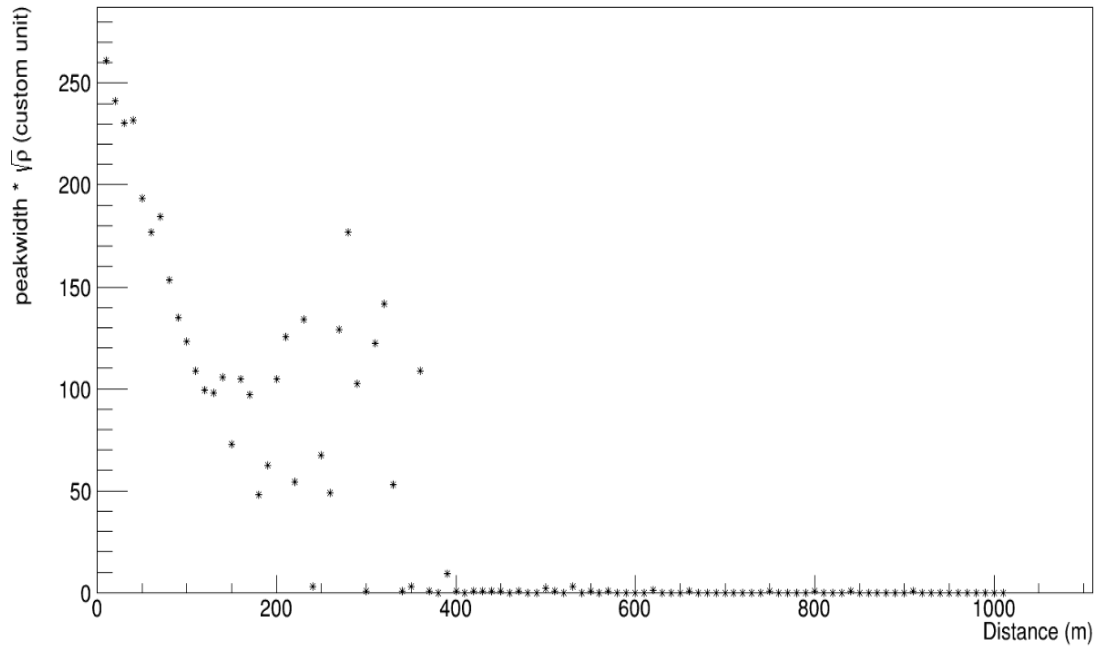


Figure 3-10: Test on  $\rho^{0.5}(R) * \tau(R)$  for EAS arriving at the detector of size  $2 \times 2 m^2$  [3].

# Chapter 4

## Experiment Physics Run 1

### 4.1 HorizonT detector system

HorizonT detector system (HT) is a cosmic rays detector system located at the high-altitude level ( $\sim 3500$  meters above sea) in the Tian Shan mountains near Almaty, Kazakhstan. HT is a part of Tian Shan High-altitude Science Station (TSHASS) of Lebedev Physical Institute of the Russian Academy of Sciences. It is designed to study EAS with the energy range of  $\sim 10^{16} - 10^{19}$  and a wide zenith angle interval ( $0^\circ - 85^\circ$ ) [11, 12]. Aerial view of HT detector system is presented in Figure 4-1 [13].



Figure 4-1: Top view of Horizon-T detector system.

There are three Vavilov-Cherenkov radiation detectors and eight charged particles(scintillator and glass) detection points that are separated by the distance of around of hundreds meters. In the table 4-1, the distances from the coordinate positions of the detection points to the Central detection point are presented. The distance between the farthest detectors is up to 1 kilometer.

Table 4.1: HT detector points coordinates.

<b>Station</b>	<b><math>X, m</math></b>	<b><math>Y, m</math></b>	<b><math>Z, m</math></b>	<b><math>R, m</math></b>
1	0	0	0	0
2	-445.9	-85.6	2.8	454.1
3	384.9	79.5	36.1	394.7
4	-55.0	-94.0	31.1	113.3
5	-142.4	36.9	-12.6	147.6
6	151.2	-17.9	31.3	155.4
7	88.6	178.4	-39.0	203
8	221.3	262	160.7	374

At HT detector system, each detector connects to the Data Acquisition system located at the detection point 1 (Center) via cables. SC detectors are calibrated using their response signal from minimally ionizing particles (MIP) of the cosmic rays flux. In this thesis, the calibration of the time delay in each cable and the signal loss is taken into account as well as their MIP response values [14, 15].

Each scintillator (SC) detector is a square-shaped polystyrene scintillator cast of the  $1 m^2$  area and 5 cm width [15, 11]. In this thesis, SC detectors are considered only. Scintillator is a material, in which charged particles passing through it excite electrons in it that are de-excite mostly with photon emission. The output of SC detectors is proportional to the number of particles. Thus, SC detectors can be referred to counters [16]. Light is registered by PMT that is placed above the center of detection medium at the height 1 m for scintillator and 0.5 m for glass.

Each detection point has both SC and GD detectors equipped with 2 types of photomultiplier tubes (PMT) [11]. SC and GD detectors are equipped with Hamamatsu R7723 PMT [17, 12] assembly, plastic scintillator with MELZ FEU49 PMT [18, 12], glass with R7723 PMTs and also Vavilov-Cherenkov radiation detector equipped both

with Hamamatsu H6527 PMT and FEU49 [12].

Figure 4-2 illustrates schematics of SC detector including scintillator material, PMT and ADC and the basic operation showing that detected photons passed through PMT converted into electric pulses that are amplified, digitized and then sent to PC.

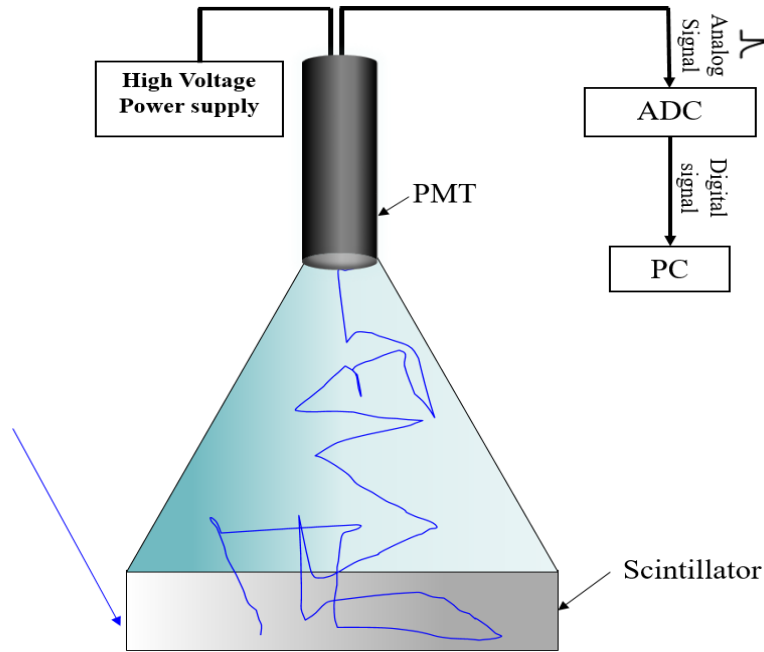


Figure 4-2: Illustration of basic SC detector operation.

SC detectors response were calibrated (see Appendix A) using MIP (minimally ionizing particle) including uncertainty caused by loss and widening of a signal in cables.

## 4.2 Data analysis and classification

In Chapter 3, such EAS characteristics as particle density, arrival time, passage time difference (width of EAS disk), distance from the disk axis and their relations were defined. Unlike simulation, information on the type and energy of primary particle is not known, only data of arrival time and number of particles are available. In this chapter, these EAS features will be used in study of experimental data and validation of invariant property of EAS predicted in simulation.

Around 2000 events with EAS were selected from the total set of events that has been detected during the period from January 2017 to April 2017 at the Horizon-T detector system. The passage of charged through scintillator detectors is registered with accuracy of 20 ns.

### 4.2.1 Standard EAS

At energies below  $10^{16}$  eV, EAS events detected at HT detector system have similar pulse shape structure with single modes, which will be called in the thesis as "standard" events. According to the analysis, the main important information of longitudinal development of the shower in the atmosphere is contained in the first half of the pulse over a time interval from  $t_{0,1}$  to the median  $t_{Me}$ . The pulse front side is steeper than its back side.

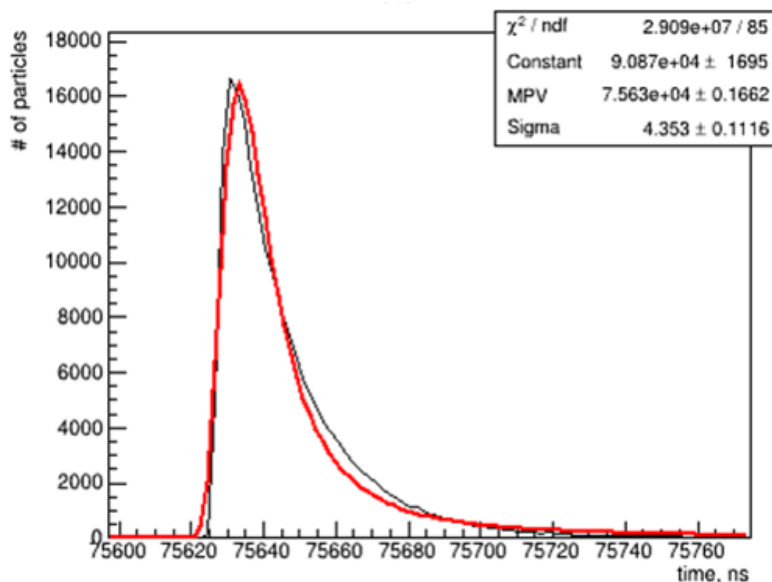


Figure 4-3: Single pulse of EAS detected at HT detector system.

Sample of standard event, registered on April 11 2017 year at 13:46 UTC is demonstrated in Figures 4-4 and 4-5. It is seen that the shower axis passed from the side of detector Upper and arrived close to the Center detection point, where the highest peak is displayed. In Figure 4-5, five peaks registered at five detection points (Upper, Right, Left, Kurashkin and Bottom) are shown.

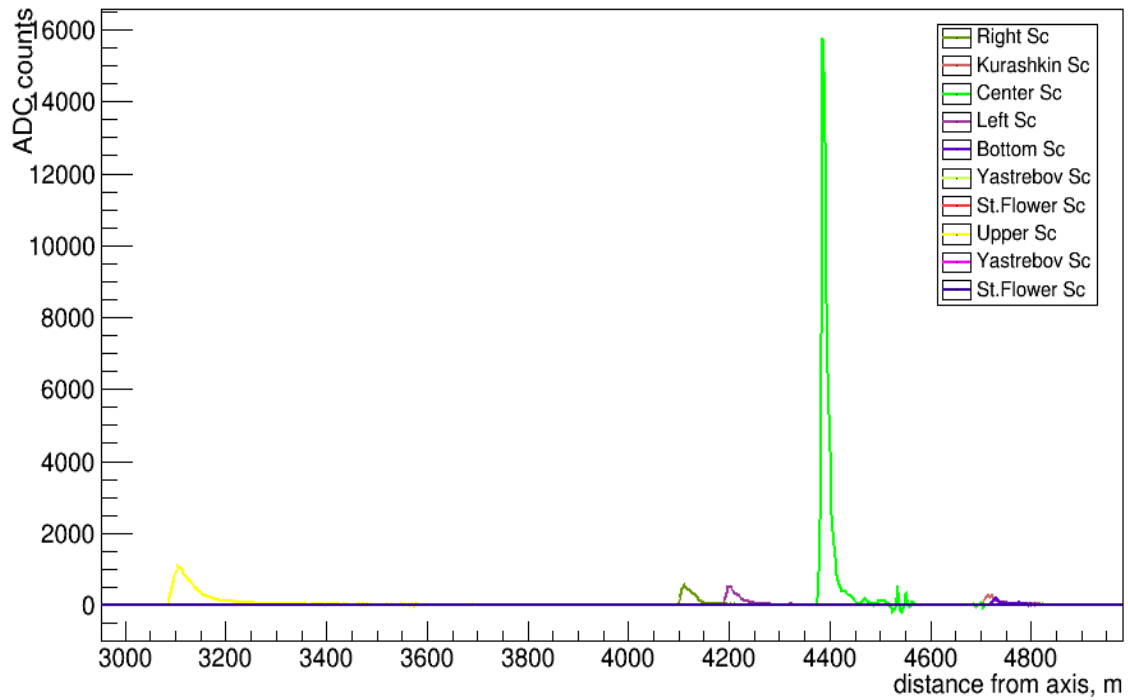


Figure 4-4: Standard EAS event with all detector channels displayed.

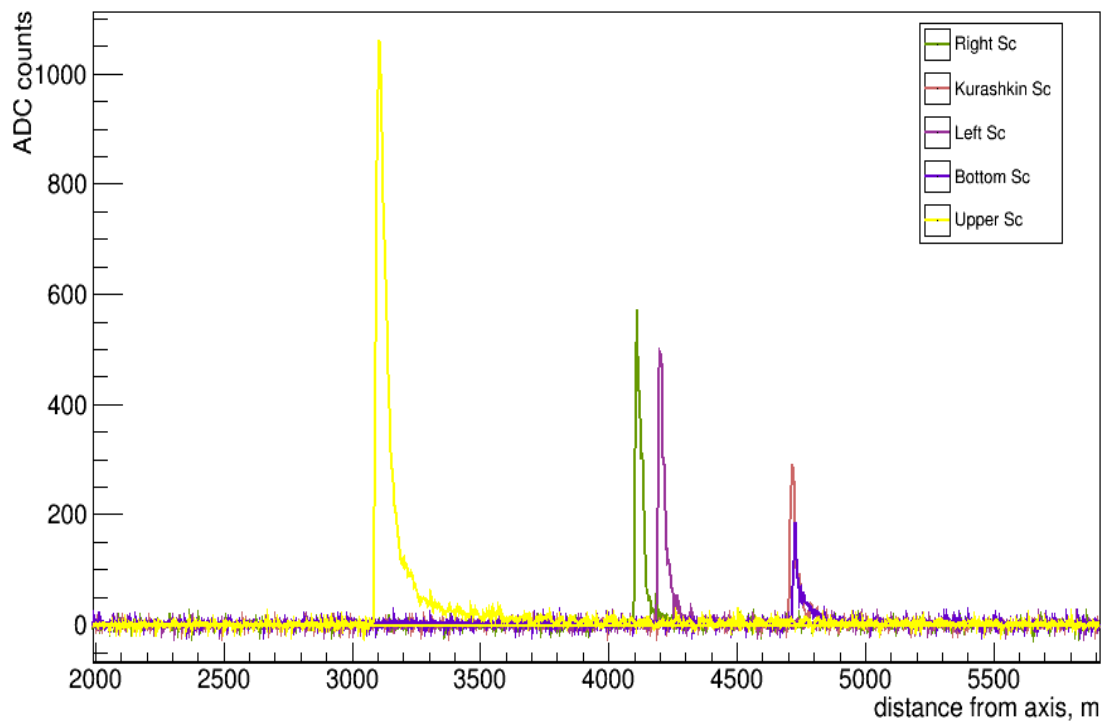


Figure 4-5: Standard EAS event without highest peak displayed.



All pulses have a single-mode smooth shape that does not vary with the distance from the EAS axis. From the analysis results, it is seen that peak area or particle density in MIP drops as  $1/r^2$  at the  $\sim 150$  meters from the axis (see Figure 4-6). Figure 4-7 demonstrates linear increase of the peak width or the width of the EAS disk with the distance from the axis.

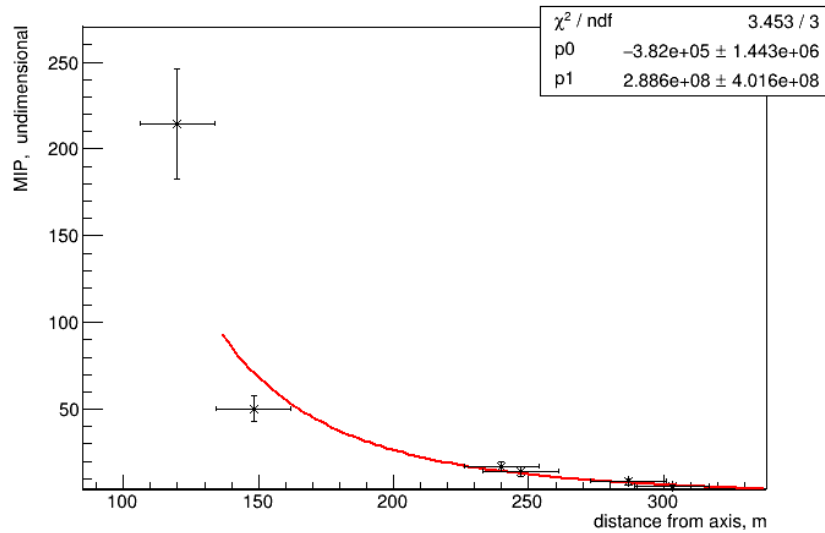


Figure 4-6: Peak area or density of particles vs. the distance from the EAS core.

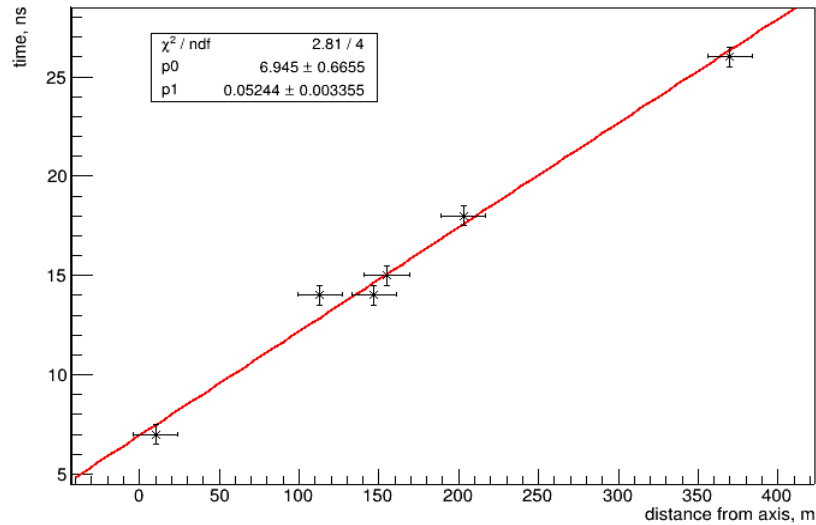


Figure 4-7: Peak width vs. distance from the EAS core.

The analysis confirms that the standard EAS have the same properties as simulated ones.

## 4.2.2 Testing and verification of simulation results on data

First, selected data were analyzed by programming code written specifically for this purpose. Each individual pulse corresponding to a single SC detector was considered separately.

In the analysis, particle density, arrival time values and their difference were used. Particle density of EAS is taken as a pulse area, which is defined as integral of 0.1 and 0.5 of the total area under the pulse.

In the previous section, EAS simulated by CORSIKA are defined as standard. Section 3.2 discusses the results of analysis of simulated EAS, which predict a certain characteristic that is invariant for the EAS of specific energy. The main purpose for the search of invariant properties of EAS is to use them as them in methodology of EAS data analysis. Thus, the observed invariant property was tested in standard EAS obtained from data.

From the total number of  $\sim 2000$  EAS events collected in Physics Run I, approximately 500 can be defined as standard. For the analysis purpose, the data was chosen of high quality only with clear standard pulse shape. Around 50 standard EAS events were tested on the invariant property is defined as  $\rho^{0.5}(R) * \tau(R)$  and predicted by simulator. After calibration, the value

$$MIP^{0.5}(R) * \tau(R) \tag{4.1}$$

was calculated and used in this analysis.

Since uncertainties due cable and detector effects are uncluded in MIP calibration for each SC detector, the error was calculated simply as fractional uncertainty.

## Results

The Analysis showed that for almost all selected events the property  $MIP^{0.5}(R)*\tau(R)$  is not invariant. Figure 4-8 demonstrates this result on the sample of standard EAS detected on March 05 2017 at 08:05 UTC. Obviously, there is no evidence of any invariant properties. According to simulation results, invariance is observed on the

distance from the EAS axis between 200 and 450 meters. However, on the data sample (Figure 4-9) the radius of EAS disk is around 230 meters, which corresponds to the approximate estimate of EAS energy of  $10^{15} eV$ .

Figure 4-9 shows the analysis result for the another sample data of EAS recorded on April 12 2017 at 13:27 UTC. This result is more interesting as the radius of the EAS disk is  $\sim 300$  meters with the corresponding the energy about  $10^{16} eV$ . It can be seen that the spread of  $MIP^{0.5}(R) * \tau(R)$  is not as large as in the previous result ( $\pm 20$ ). This is the best result, which was demonstrated only for the one sample of EAS. Thus, it cannot be considered as invariant.

In the data, standard EAS are observed at the energies lower than  $10^{16} eV$ . EAS of these energies develop disks of radii up to 200-250 meters. HT detector system has sparse configuration with the separation between detectors from  $\sim 100$ -400 meters, which can be not enough to detect full EAS disks of relatively small energies ( $< 10^{16} eV$ ). This can explain the luck of evidence of the studied invariant property in data.

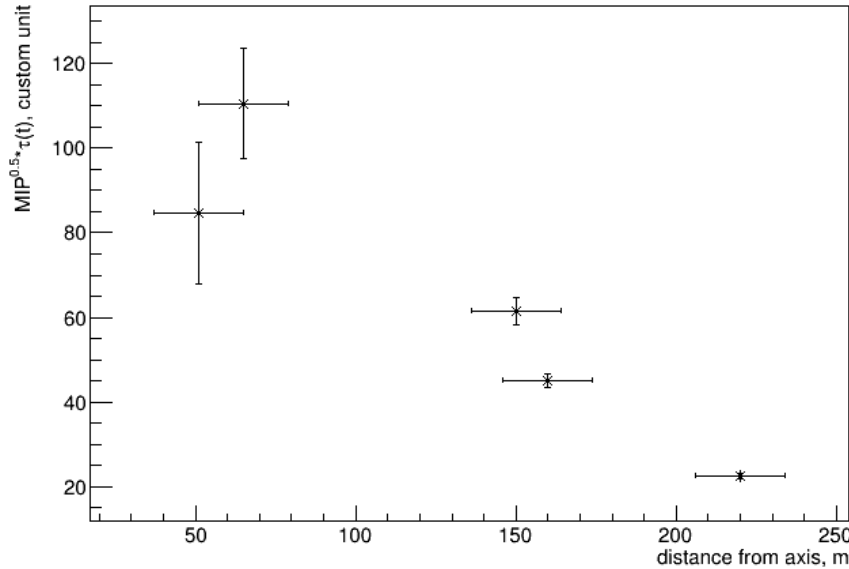


Figure 4-8: Test on invariance of  $\rho^{0.5}(R) * \tau(R)$  in EAS event

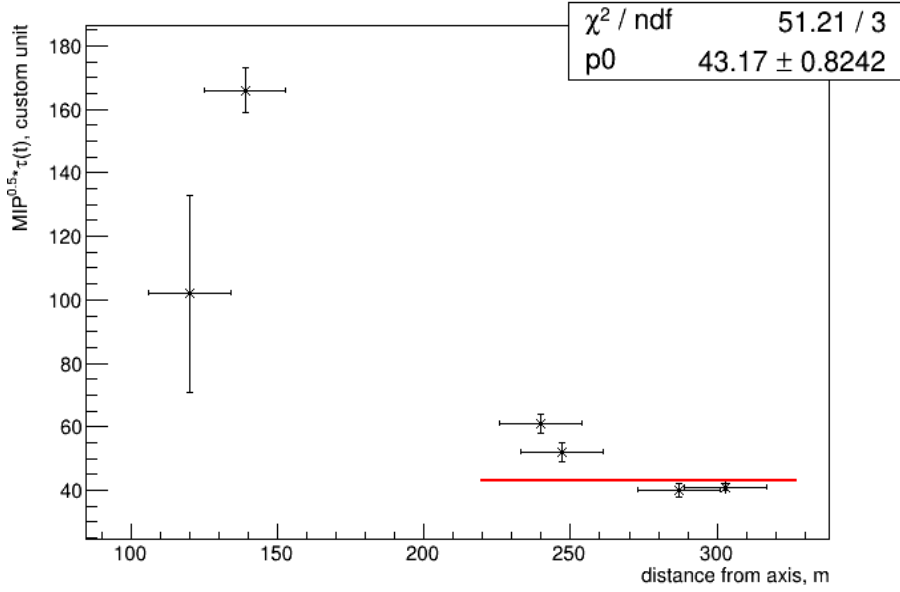


Figure 4-9: Test on invariance of  $^{0.5}(R) * \tau(R)$  in EAS event.

### 4.2.3 Multimodal EAS

Among the data, many unusual EAS, whose charged particle fluxes caused pulses with several peaks (modes), were discovered. These multiple peaks are observed at the detection points located at distances of hundreds of meters from each other. Further these events will be called multimodal EAS (MME). MME events are usually observed at energies above  $10^{17}$  eV.

Pulses with several modes were first recorded by the English physicist J.V. Jelly [19]. In subsequent years, events with multimodal impulses were recorded by many researchers. In the past, these researchers explained such events by the birth of particles with very large masses, which lag behind the main shower disk. They believed that the secondary particles originated from such heavy particles propagated through atmosphere with delay compared to the main EAS. Therefore, events with multimodal impulses were called events with delayed particles.

In unusual EAS, it is unclear which of the modes of multimodal pulses recorded at different detection points can be taken to determine the shower axis. Therefore, we use the concept of the axis conditionally, when the shower axis is determined from the time of passage through the installation.

Sample of a multimodal EAS event registered at the Horizon-T detector system on February 11 2017 year at 05:20 UTC is shown in Figures 4-10, 4-11 and 4-12 .

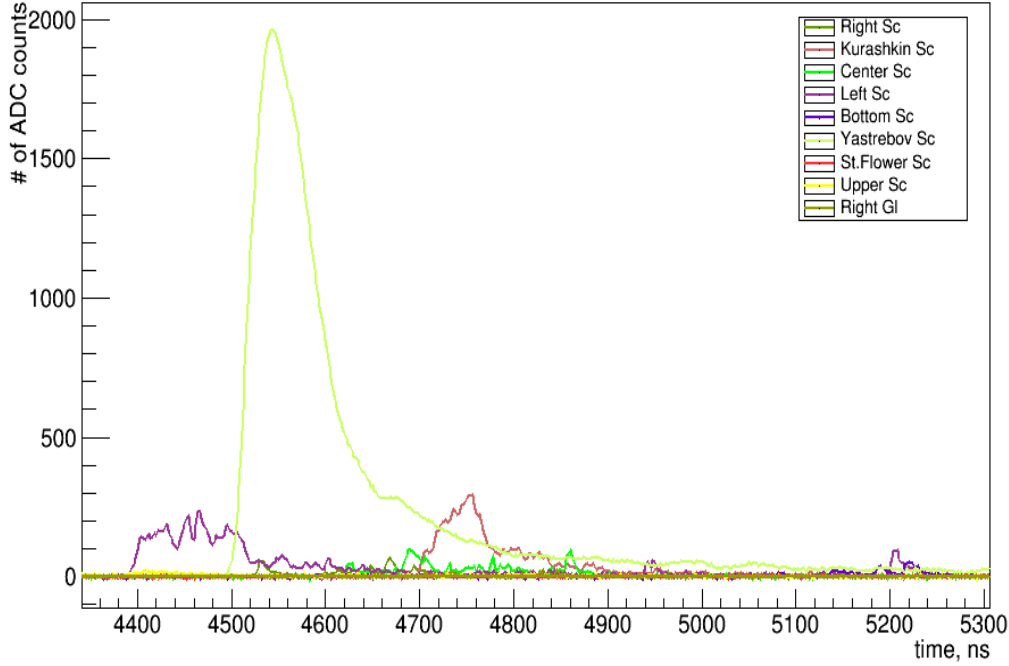


Figure 4-10: MME detected by HT detector system with all channels displayed.

Figure 4-10 displays all pulses of the event. You can see the very large pulse at detection point 2 indicating that the axis arrived closer to the detection point 2; and the next two pulses visible at detection points. The rest pulses are much smaller than the pulse 2, so they are practically not visible in the figure. The pulse from point 2 has a shape of standard EAS that deviates from that of visible pulses at the other 2 points.

The peaks with smaller amplitudes have complex broken pulse structure that is tend to split (see Figure 4-11). These peaks are visible at the Kurashkin and Left detection points at relatively same distance from the axis.

Figure 4-12 displays 2 peaks with multimodal structure. They are located at the farthest location from the EAS axis and separated from each other by hundreds of ns.

In this EAS event, all detection points of HT detector system recorded pulses,

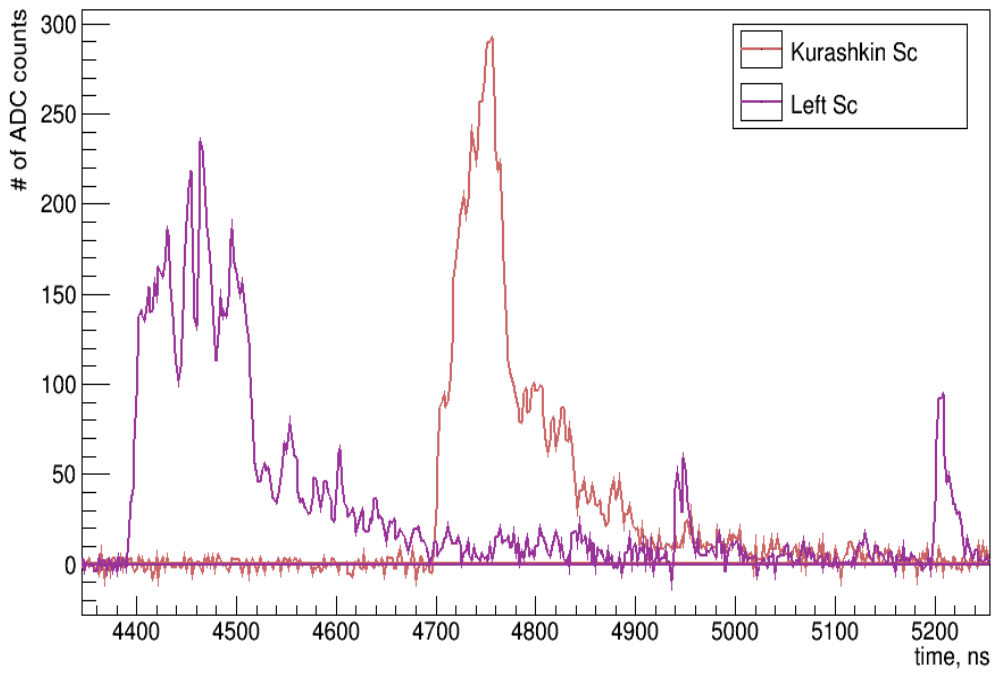


Figure 4-11: MME detected by HT detector system at  $\sim 300$  meters from axis.

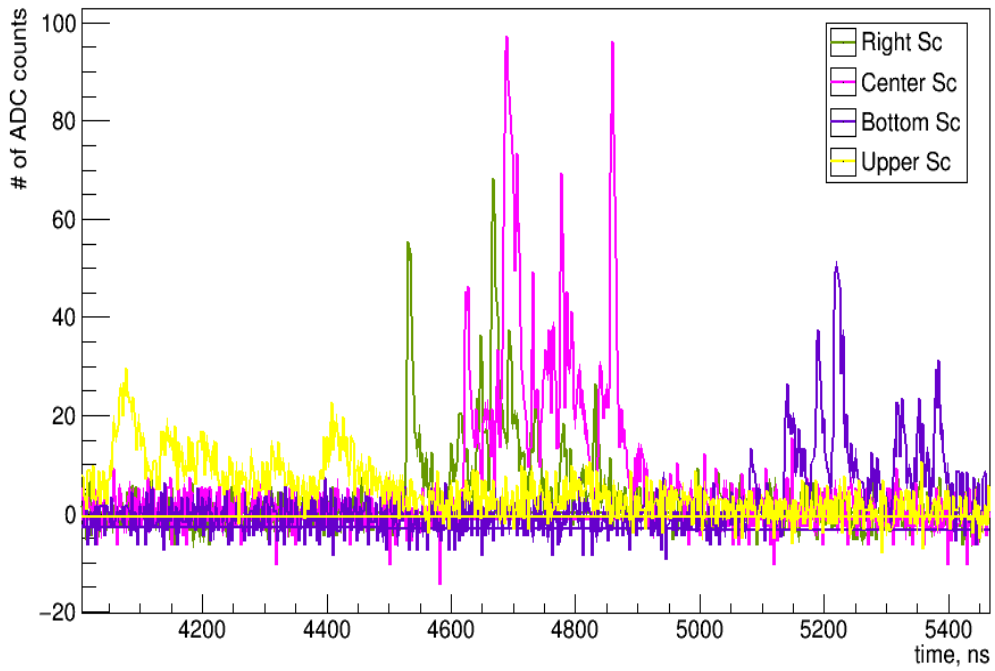


Figure 4-12: MME detected by HT detector system at  $\sim 500$  meters from axis.

which means that the the radius of the EAS is at least 1 km. The approximate estimate of energy of this EAS event is above  $10^{17}$  eV.

Another example of such MME is given below. The event in Figure 4-13 was detected on April 8 2017 year at 12:26 UTC.

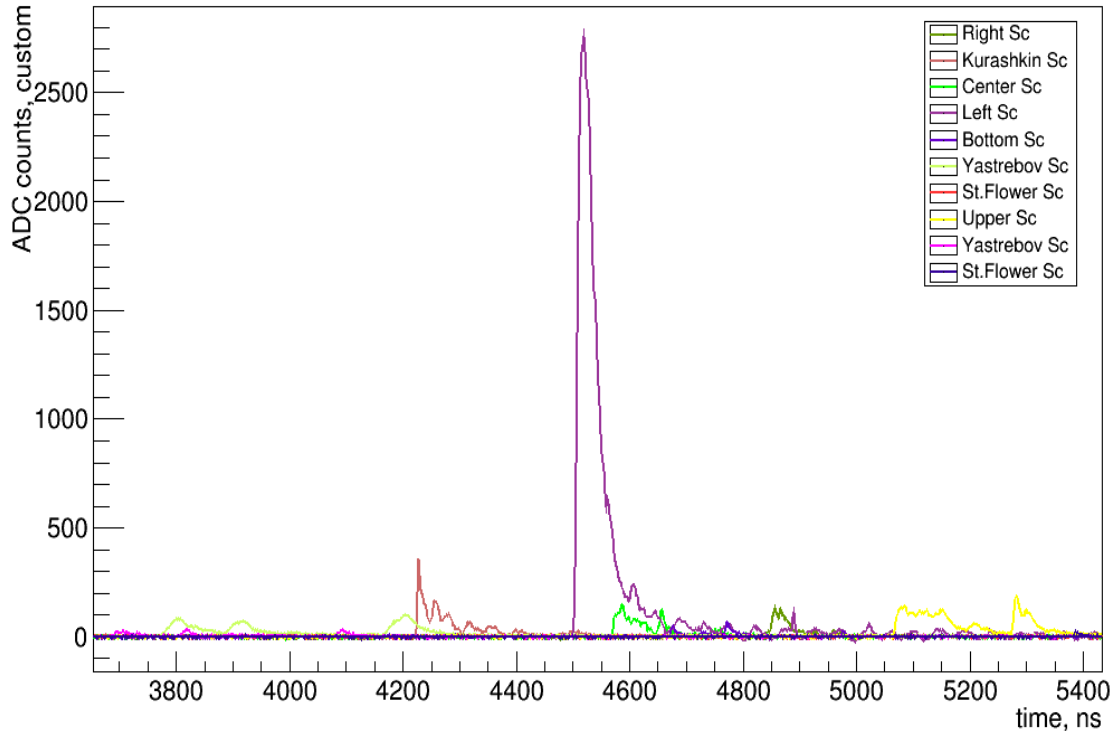


Figure 4-13: Sample MME event with all channels displayed.

From the EAS display, the very large signal is visible at the Left detection point, indicating that the EAS has arrived close to the this point. Since the amplitudes of pulses registered at other detection points are much smaller compared to the largest, they are not visible on the display. Note that the largest peak has smooth shape as Standard EAS. The next pulses that are closer to the axis (Kurashkin, Right, Center) start to deviate from the smooth shape. They are located at approximately same distance from the EAS axis (Left detection point).

The pulses from the Yastrebov, Bottom and Upper detection points demonstrate complex multimodal shape. Both two pulses (red and blue) of Yastrebov detector station, where two SC detectors are located, display similar 3-modal structure. The pulse from the Bottom detector station repeats this 3-modal shape. The peaks are

separated by hundreds of ns from each other.

From the detection configuration, it can be concluded that the radius of the EAS event is  $\sim 1$  km. Thus, the event is the very high energy EAS event ( $\geq 10^{17} eV$ ). In Appendix B, two other samples of such MME events are given.

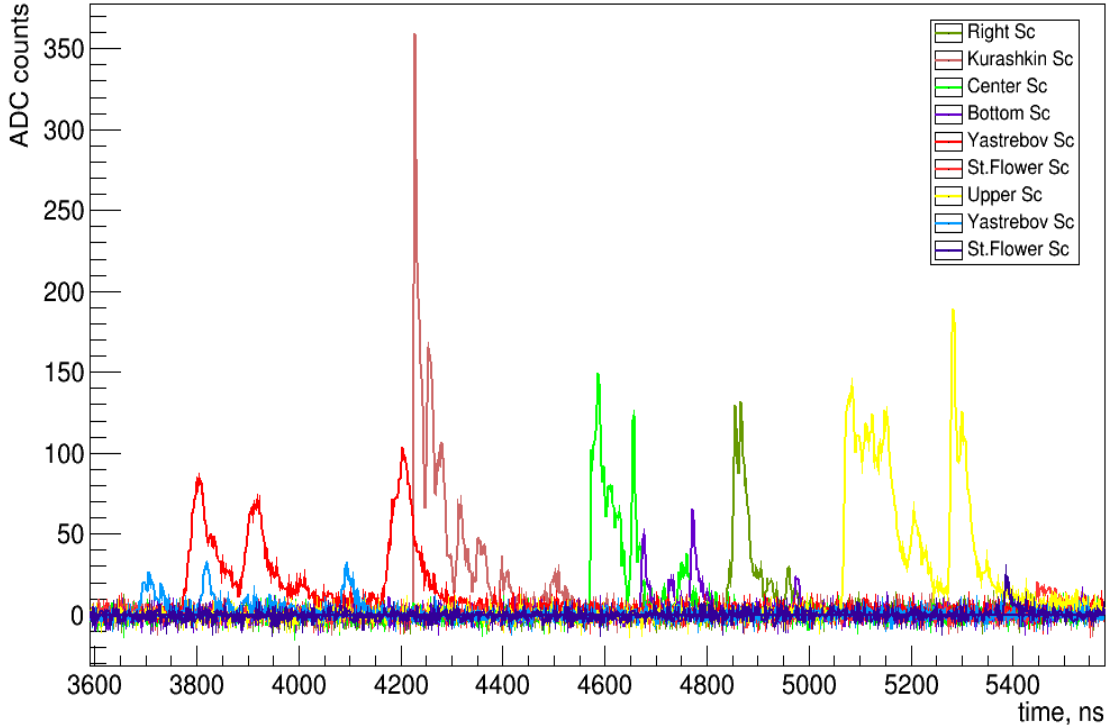


Figure 4-14: Sample MME event without largest peak.

#### 4.2.4 Statistics

Among the data detected during Physics Run I of the HT detector system operations, two main types of EAS were observed. The type of EAS events with properties familiar from simulation output are classified as ordinary or later called "standard".

The second type of events, constantly detected at TSHSS, is unusual, the nature of which can not yet be explained. The EAS events of this type were named as Multimodal EAS (MME). The phenomenon of this events can indicate on an unknown nature of particles themselves or processes that emerge in the atmosphere.

In Figure 4-15, statistics of the detection of both types of EAS events is shown



relative to their approximate energies.

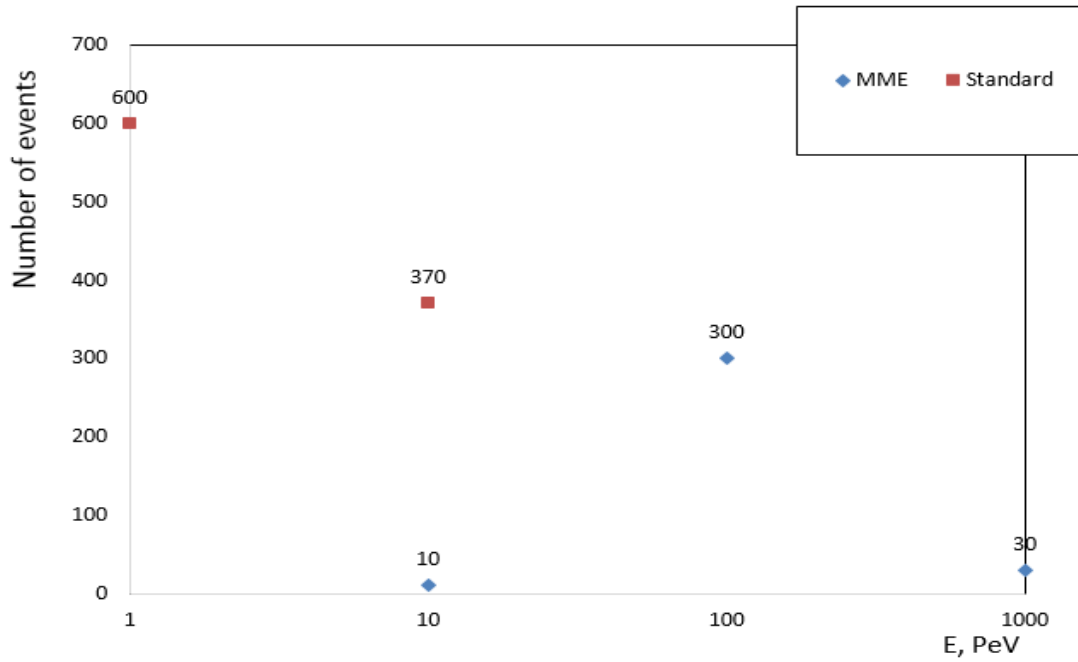


Figure 4-15: Statistics of MME and Standard EAS events detected at HT detector system.

At energies higher than  $10^{16}$  eV, only MME events are observed. Standard EAS events are observed at energies  $\leq 10^{16}$  eV.

# Chapter 5

## Conclusion

Cosmic rays are detected and studied through EAS they produce in the Earth atmosphere. Horizon-T detector system (HT) is located at the high-altitude in Tien Shan mountains (3340 meters above sea) and designed to measure spacial and temporal structure of EAS. HT system operates using 8 scintillator detectors each of  $1 \times 1 \text{ m}^2$  size. The detector time resolution is  $6.1 \pm 0 \text{ ns}$ . The detection rate of EAS with energy above  $\sim 10^{16} \text{ eV}$  is about 7 events/hour.

In this thesis, EAS were studied through analysis of experimental data obtained during experiment Physics Run I and simulation with CORSIKA. The main aim of this study was to investigate EAS detected at the HT detector system and find properties that can be used in an experimental methodology as a new approach to study EAS.

From the theory of EAS, it was suggested that there is a possible invariant property that can be used as characterization of EAS, and consequently as a new method in data analysis. This invariant property was described in Chapter 3. First, existence of this property was tested on simulated EAS. Simulation was obtained for 10 EAS of primary cosmic ray particles (Fe and proton) of energies  $10^{17} \text{ eV}$  with the variation of arrival angle and size of detector. Results showed that invariance observed for the detector size of  $10 \times 10 \text{ m}^2$  and larger, and clearly appeared at the certain distance interval from EAS axis (200 - 450 meters). It was also shown that the invariance is observed regardless of the zenith angle of EAS arrival and the type of a primary

particle.

Data of  $\sim 2000$  EAS events obtained in Physics Run I were analyzed, studied and compared with simulation. I was aiming to study characteristics of EAS and verify existence of invariant property suggested by theory and simulation in data.

As the result of data selection and analysis, many EAS detected at HT system appeared to be very interesting. In the data, EAS events that could be analyzed and characterized using information from EAS theory were classified as standard EAS events. The important fact is that standard EAS events are observed at the energy range starting from  $10^{16}$  eV and less. The other important classification factor was pulse shape of EAS events registered at each SC detector. According to this, pulse shape of standard EAS is smooth and importantly - single-mode. According to the analysis, standard events have same properties as EAS simulated by CORSIKA. Thus, theoretical suggestion about the EAS invariant property that was confirmed by simulation, was tested only on standard EAS events. As the result of this study, invariant property was not confirmed in data in standard EAS events data .

Obviously, there are other EAS types that were subjected to classification. The most interesting EAS type was classified as multimodal events. These EAS were observed at the energies higher than  $10^{17}eV$  that corresponds to radii of EAS disks starting from  $\sim 500$  meters and much larger. The distinctive feature of multimodal EAS is a complex pulse shape structure consisting of several pulse peaks. Multimodal EAS are observed at energies higher than  $10^{17}$  eV. This indicate that rest mass of a primary particle exceeds  $10^{12}$  eV. Existence of such particle contradicts gauge invariance theories. Thus, these EAS events are very interesting and may indicate on a new physical phenomenon. Currently, our research team focuses on the study of multimodal EAS.

# Appendix A

## Tables

Detector MIP response pulse area at operating bias voltage.

Detection point and cable designation	Detector type	Area (ADC counts·ns )
Bottom New	SC	$529 \pm 91$
Center Yellow	SC	$470 \pm 57$
Left New	SC	$574 \pm 110$
Right New	SC	$513 \pm 78$
Stone Flower New	SC/FEU49	$529 \pm 91$
Yastrebov New	SC/FEU49	$2200 \pm 429$
Upper New	SC/FEU49	$768 \pm 124$
Kurashkin New	SC	$549 \pm 107$

# Appendix B

## Figures

Sample of MME event detected on March 8 2017 at 14:41 UTC (see Figure B-1).

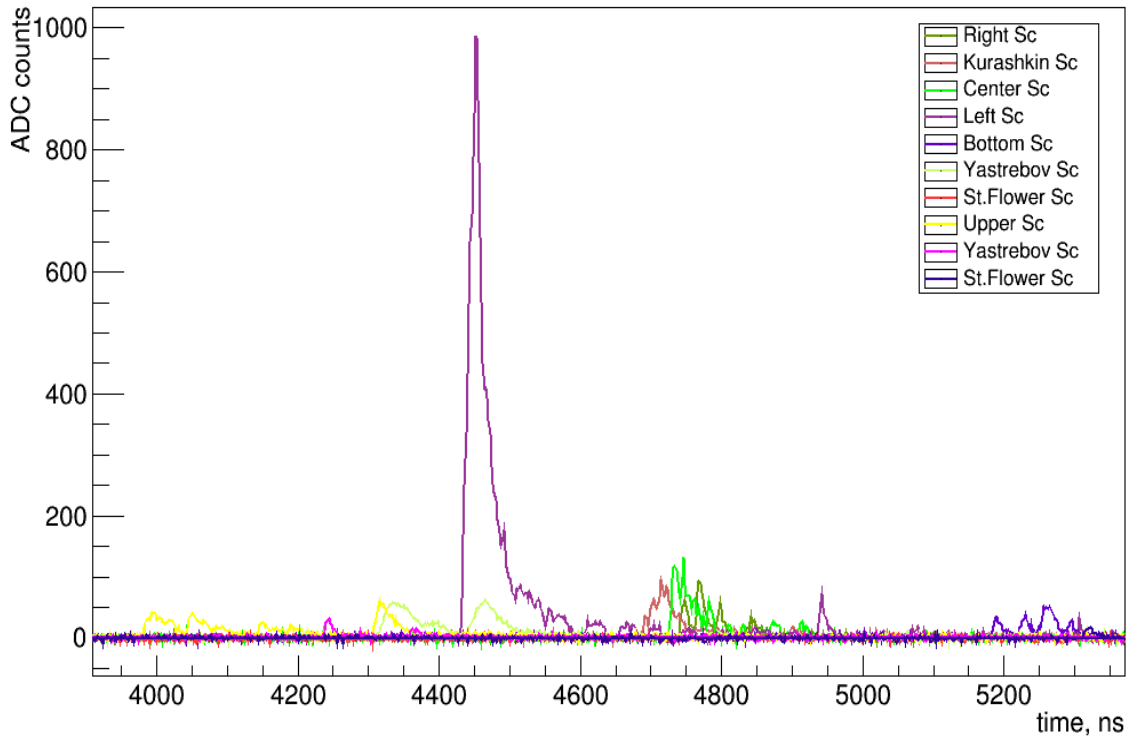


Figure B-1: Sample of MME event with all channels displayed.

In Figure B-3, MME event was detected on February 13 2017 at 22:05 UTC at the HT detector system. This is the partial event, because the largest peak (Left detection station) has the pulse structure that deviates from the standard smooth

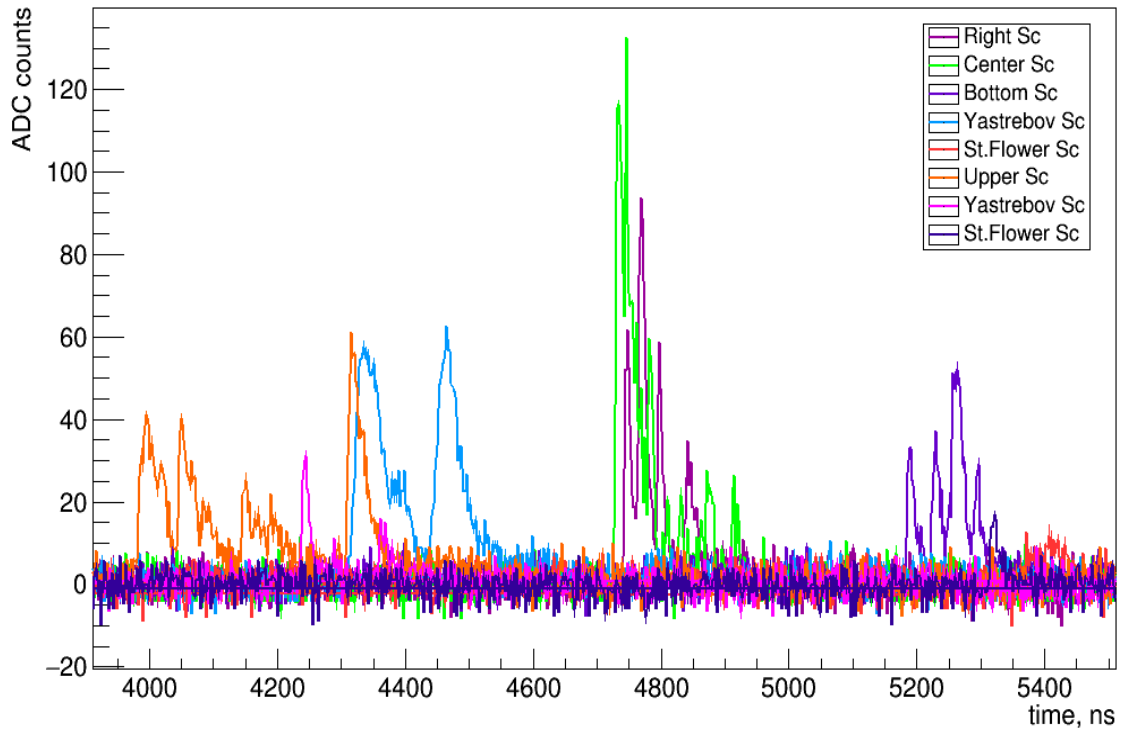


Figure B-2: Sample of MME event without largest peak.

shape.

In Figure B-4, pulses of the given MME event demonstrate complex shape. Pulses at Kurashkin, Center and Right detection points have structure that is tend to split. Pulse registered at the Upper and Bottom detection points demonstrate multimodal structure with peaks separated by several hundreds of ns.

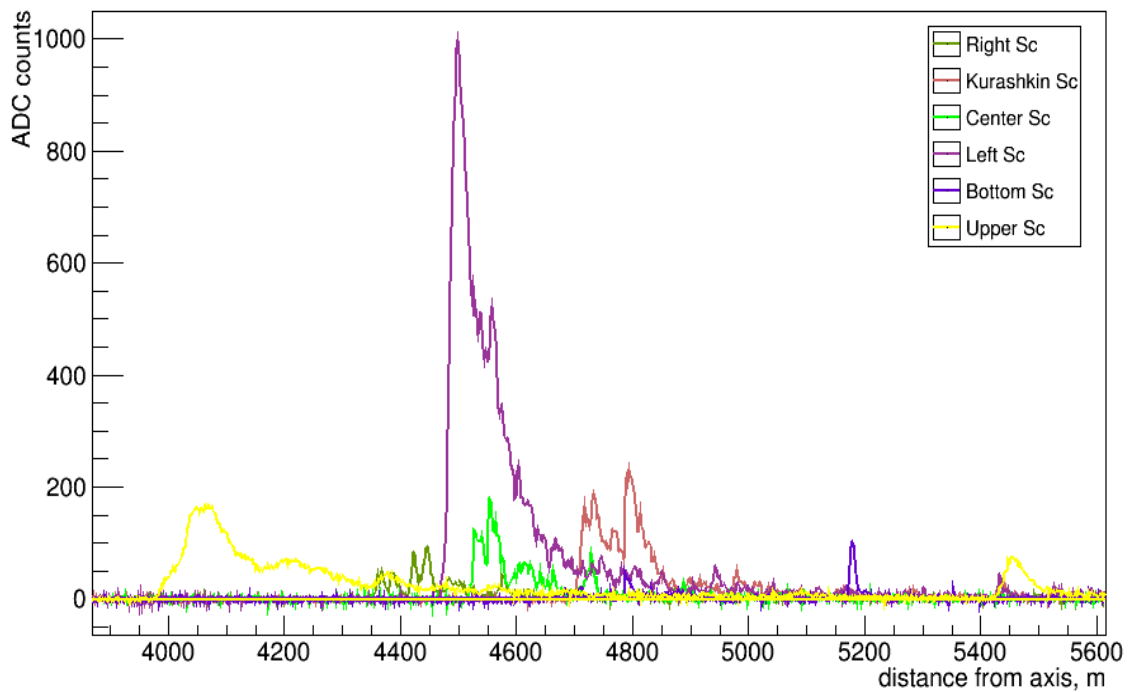


Figure B-3: Sample of MME with all channels displayed.

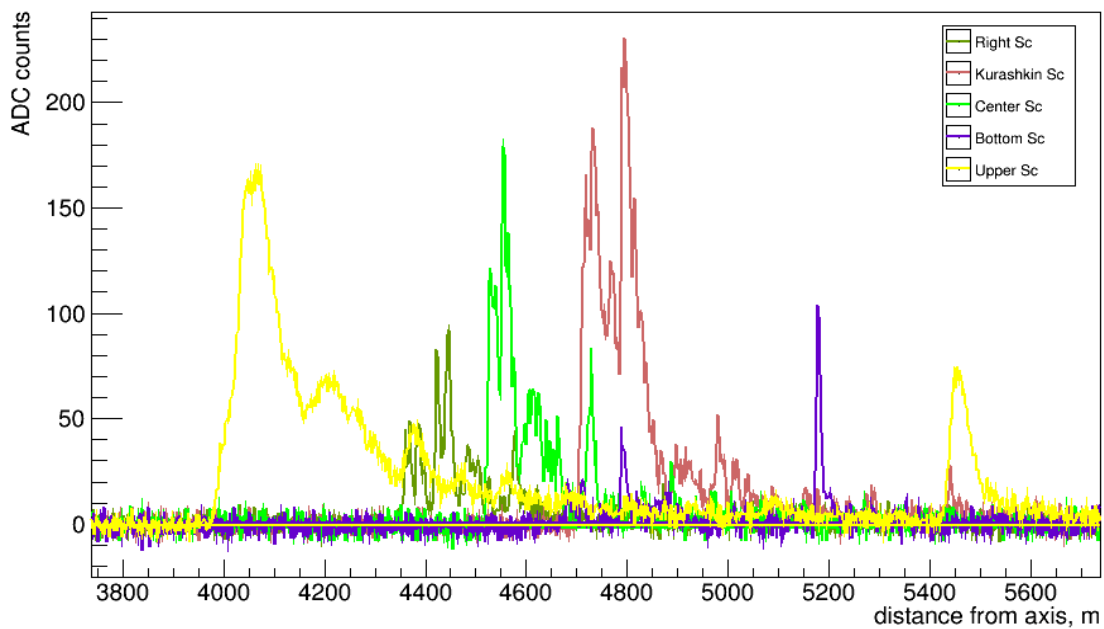


Figure B-4: Sample of MME event without largest peak.

# Bibliography

- [1] P. K. Grieder, Extensive Air Showers. High Energy Phenomena and Astrophysical Aspects. A Tutorial, Reference Manual and Data Book, vol. 1. Berlin, Heidelberg: Springer, 2010.
- [2] J. D. Haverhoek, “Ultra high energy cosmic ray extensive air shower simulations using corsika,” 2006.
- [3] A. Konysbayeva, “Using pulse shape information for individual extensive air showers (eas) analysis for simulation,” master’s project, Nazarbayev University, Physics Department, 2017.
- [4] V. Hess, “Durchdringende strahlung bei sieben freiballonfahrten,” Zeitschrift für Physik, vol. 13, p. 1084, 1912.
- [5] J. Blümer, R. Engel, and J. Hörandel, “Cosmic rays from the knee to the highest energies,” Progress in Particle and Nuclear Physics, vol. 145, pp. 293 – 338, 2009.
- [6] W. Bothe and W. Kolhöster, “Das wesen der hâhenstrahlung,” Zeitschrift für Physik, vol. 56, pp. 751–777, 1929.
- [7] J. Matthews, “A Heitler model of extensive air showers,” Astroparticle Physics, vol. 22, no. 5, pp. 387 – 397, 2005.
- [8] D. Heck, Forschungszentrum Karlsruhe Report FZKA 6019, 1998.
- [9] S. Shama and Vishwamittar, “Brownian motion problem: Random walk and beyond,” RESONANCE, 08 2005.
- [10] R. Beisembaev, “Problems related to ultrahigh-energy particles in physics and astrophysics,” in Fourth International School for young scientists from CIS, 2017.
- [11] D. Beznosko, R. Beisembaev, E. Beisembaeva, A. Duspayev, A. Iakovlev, T. Sadykov, T. Uakhitov, M. Vildanova, M. Yessenov, and V. Zhukov, “Fast and simple glass-based charged particles detector with large linear detection range,” Journal of Instrumentation, vol. 12, pp. T07008–T07008, 07 2017.
- [12] D. Beznosko, R. Beisembaev, K. Baigarin, E. Beisembaeva, O. Dalkarov, V. Ryabov, T. Sadykov, S. Shaulov, A. Stepanov, M. Vildanova, N. Vildanov, and V. Zhukov, “Extensive air showers with unusual structure,” vol. 145, p. 14001, 01 2017.



- [13] R. Beisembaev, E. A. Beisembaeva, O. Dalkarov, V. A. Ryabov, A. V. Stepanov, N. G. Vildanov, M. I. Vildanova, V. Zhukov, K. A. Baigarin, D. Beznosko, T. X. Sadykov, and N. S Suleymenov, “The Horizon-T experiment: Extensive air showers detection,” 05 2016.
- [14] D. Beznosko, T. Beremkulov, A. Iakovlev, S. Jakupov, D. Turganov, A. Tusipzhan, T. Uakhitov, M. I. Vildanova, A. Yeltokov, and V. Zhukov, “Horizon-T experiment upgrade and calibration of new detection points,” 03 2018.
- [15] D. Beznosko, T. Beremkulov, A. Iakovlev, A. Duspayev, M. I. Vildanova, T. Uakhitov, K. Yelshibekov, M. Yessenov, and V. Zhukov, “Horizon-T experiment calibrations - mip signal from scintillator and glass detectors,” 03 2017.
- [16] A. Baitenov, A. Iakovlev, and D. Beznosko, “Technical manual: a survey of scintillating medium for high-energy particle detection,” 01 2016.
- [17] Hamamatsu Photonics, (<http://www.hamamatsu.com>, Shimokanzo, Toyooka-village, Iwatagun, Shizuoka-ken, 438-0193 Japan).
- [18] MELZ-FEU, (4922-y pr-d, 4c5, Zelenograd, Moskva, Russia, 124482).
- [19] J. Jelly and W. Whitehouse Proceedings of the Physical Society, A66, 454 , 1953.